Cavitation bubble dynamics in microfluidic gaps of variable height

Pedro A. Quinto-Su, Kang Y. Lim, and Claus-Dieter Ohl
Division of Physics and Applied Physics, School of Physical and Mathematical Sciences, Nanyang Technological University, Singapore 637371, Singapore

(Received 12 July 2009; published 6 October 2009)

We study experimentally the dynamics of laser-induced cavitation bubbles created inside a narrow gap. The gap height, h, is varied from 15 to 400 μm and the resulting bubble dynamics is compared to a semiunbounded fluid. The cavitation bubbles are created with pulsed laser light at constant laser energy and are imaged with a high-speed camera. The bubble lifetime increases with decreasing gap height by up to 50% whereas the maximum projected bubble radius remains constant. Comparing the radial dynamics to potential flow models, we find that with smaller gaps, the bubble-induced flow becomes essentially planar, thus slower flows with reduced shear. These findings might have important consequences for microfluidic applications where it is desirable to tune the strength and range of the interactions such as in the case of cell lysis and cell membrane poration.

DOI: 10.1103/PhysRevE.80.047301 PACS number(s): 47.55.dp, 47.55.dd

Laser-induced cavitation bubbles have been used for a broad range of applications, among others, for example, cell lysis [1], cell membrane poration [2], ocular surgery [3], and the study of sonoluminescence [4]. Yet, it has been only until recently that this technique has been combined with microfluidic chips [5–10] which are used for the analysis and synthesis of small amounts of liquid chemicals, e.g., for biological and medical analysis [11]. Conventional microfluidic devices operate due to the small dimensions of the channels in the low Reynolds number regime where viscous surface forces dominate. Yet, in this regime, mixing and fluid pumping are difficult to achieve. Laser-induced cavitation bubbles created inside the microchannels can overcome this limitation since the induced flow by the rapid bubble dynamics can reach speeds of several meters per second. Furthermore, the induced flow stops almost immediately after the bubble collapses (microsecond time scale), which can be used to actuate the flow on these brief moments. As there is only the need for optical access to the fluid, the implementation of the technique is simple with little requirements on the designs and a remotely powered device. These advantages stimulated research and soon microfluidic handling with laser-induced cavitation has been demonstrated for pumping [6], mixing [7], cell membrane lyseing [8,9,12], and switching [10]; all these can even be digitally controlled [13].

Constraining a cavitation bubble in microfluidic devices affects the flow field and thus the strength of the flow actuation. Here, we present a fundamental study on the importance of the height of the microfluidic environment on the bubble oscillation. The bubbles are created with a fixed laser energy inside a narrow gap ranging from 15 to 400 μm. Their dynamics is recorded with a high-speed camera together with the bubble's acoustic emission using a hydrophone. The bubbles are created with a tightly focused laser pulse which explosively vaporizes the liquid due to stress confinement (see references in [13]).

The experimental setup is shown in Fig. 1. It consists of an inverted microscope (Olympus IX-71) with a 20× objective (numerical aperture=0.7) that is used to image the sample and to focus the laser pulse into the liquid gap. The laser is a frequency doubled Nd:Yttrium Aluminum Garnet (Nd:YAG) (λ=532 nm) with a pulse duration of 6 ns. The beam is expanded with a telescope consisting of two lenses (not shown) in order to fill the back aperture of the microscope objective. The narrow gap is illuminated from the top through the condenser of the microscope and the events are recorded with a high-speed camera (Photron SA-1) at 450 000 frames per second (fps) with an exposure time of 1 μs. A hydrophone (1 mm diameter needle hydrophone, Precision Acoustics, U.K.) coupled with ultrasound gel to the upper cover slip picks up the acoustic transients emitted during the bubble creation and collapse. The time interval between these two events determines the period of the bubble oscillation, T_{osc}.

The microfluidic gap is created between a couple of cover slides separated with spacers of known height h as shown in the inset of Fig. 1. The channel is filled with yellow inkjet printer ink (Maxtec, universal ink refill, Kowloon, Hong Kong, density $\rho=1046\pm1$ kg m^{-3}, kinematic viscosity at 20 °C $\nu=2.1\pm0.2\times10^{-6}$ m^2 s^{-1}) to absorb the laser light. The geometry is described with the parameter $H=h/R_{\max}$, where $R_{\max}$ is the maximum projected radius of the bubble. Thus, H lies between 0, the ideal planar, or two-dimensional (2D) geometry and $H\rightarrow\infty$ with a semiunbounded fluid, i.e., in absence of the upper cover slip. For adjustment of the

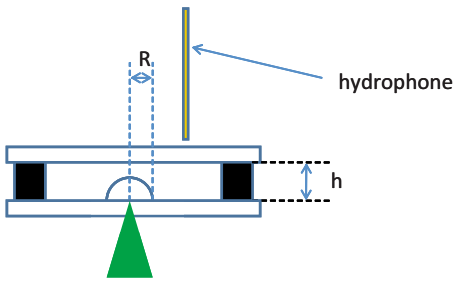

FIG. 1. (Color online) Experimental setup. A green laser pulse (λ=532 nm and 6 ns duration) is collimated and focused into a narrow gap formed by two cover slips being a distance h apart. A dichroic mirror and filter separates the laser light from the optical path of the high-speed camera (not shown). By definition, the bubble radius $R(t)$ is the projected radius imaged onto the camera.

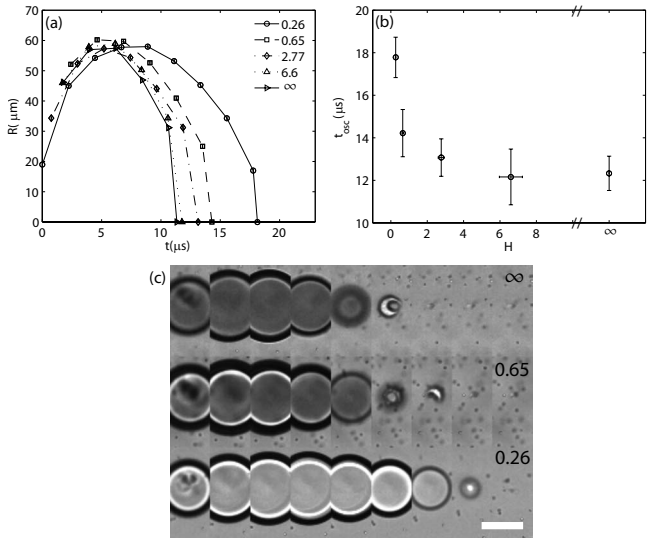

FIG. 2. (a) Radial bubble dynamics for different gap widths H, the omitted error bar for the time is ± 0.5 μs, and the standard deviation in size determined over 5 runs is ± 2 μm. (b) Lifetime of the bubble obtained from the hydrophone signal. (c) Three examples of the bubble shape seen from below for the indicated H values. The length of the scale bar is 50 μm.

laser focus just above the lower cover slip polystyrene particles with slightly higher density of the ink and 3 μm diameter are added, thus the in focus and settled particles indicate a laser focus about $1-3$ μm above the cover slip. We keep the laser energy constant for the different gap heights and create the bubble at the bottom of the lower cover slip. This way, the energy for the formation of the bubble is independent of the gap height, e.g., the bubble explodes with approximately the same initial kinetic energy. As a side note, due to the strong illumination, the liquid will become heated which reduces the viscosity; we estimate [14] an effective viscosity in the experiment of $\nu \approx 10^{-6}$ m^2 s^{-1}.

Figure 2(a) shows the radial dynamics of bubbles created in gaps with heights of 15, 40, 160, and 400 μm and one without a top glass plate, i.e., $H \to \infty$. Interestingly, all bubbles expand to approximately the same maximum radius. Yet, as displayed in Fig. 2(b), the lifetime of the bubble T_{osc} varies by about 50%; T_{osc} is shortest for $H \to \infty$ and increases with decreasing H. The shape of the bubble viewed from below is presented in Fig. 2(c) from top to bottom for $H \to \infty$, $H=0.65$, and $H=0.26$ (2.2 μs interframe time). Due to the limited pixels available at this high framing rate, only the central part of the bubble is imaged. Again, we see that the bubble collapses later with decreasing H. Additionally, for all the values of H, with the exception of $H=0.26$, some nonradial shape is observed during the last stage of collapse. We explain this shape with the formation of a jet flowing toward the bottom cover slip thereby forming a toroidal bubble [15]. The thinnest gap, $H=0.26$, shows a radially symmetric collapse on the temporal and spatial scales resolved. Interestingly, the upper two sequences depict darker-shaped bubble interiors. This may be caused by the curved bubble interface resembling a negative lens refracting the illumination light. In contrast, the narrowest gap, $H=0.26$, leads to a mainly flat, pancake-shaped bubble. The slightly brighter interior as compared to the surrounding liquid in Fig. 2(c) ($H=0.26$) is explained with a reduced absorption of light because only a very thin liquid film of the colored liquid is present at the bubble's position.

Figure 2(c) demonstrate that the fluid mechanics is rather complex, e.g., leading to curved or planar liquid-gas interfaces and the formation of jets. We now want to approximate the limiting cases of (1) a hemispherical, $H \to \infty$, and (2) a planar bubble, $H \to 0$, with potential flow models. This means that viscosity can be neglected during the expansion and collapse of the bubble. We estimate the time scale for the diffusive growth of the viscous boundary layer with $\delta t = y^2/(1.72^2 \nu)$ [14,16], where y is the vertical distance from the lower cover slip (see Fig. 1). Thus, for times shorter than $t < \delta t \approx 19$ μs, the boundary layer does not reach the center in the thinnest gap $y=7.5$ μm. Because, all bubble oscillations are shorter than 19 μs, we assume a mainly potential flow [14]. Therefore, we obtain for the hemispherical bubble case (1) the well-known Rayleigh equation [17,18]

$$R\ddot{R} + \frac{3}{2}\dot{R}^2 = \frac{P}{\rho}, \tag{1}$$

where R is the bubble radius, ρ the density of the liquid, and P is the pressure in the liquid far from the bubble. For simplicity, we neglect vapor pressure and the thermodynamics within the bubble and the liquid. The time to shrink from maximum radius, $R_{\max}$, to zero is called the Rayleigh collapse time $T_C^{3D} = 0.915 R_{\max}(\rho/P)^{1/2}$.

In contrast, the corresponding dynamic equation for the two-dimensional (cylindrical) bubble shrinkage [14,19] is

$$R\ddot{R} + \dot{R}^2 \log\frac{R}{R_\infty} = \frac{P}{\rho}. \tag{2}$$

Here, $R_\infty = 550$ μm is an experimental constant and determines the distance where the fluid velocity drops to zero, i.e., given by the experimental constrains (see Ref. [14]). The collapse time for the planar case, T_C^{2D}, can be estimated following the arguments of Chahine and Genoux [20] and we obtain $T_C^{2D} \sim T_C^{3D}[\log(R_\infty/R_{\max})]^{1/2}$. For values of $R_{\max}/R_\infty \ll 1$, the collapse phase of the cylindrical bubble is slower than a hemispherical bubble. A second difference is that the

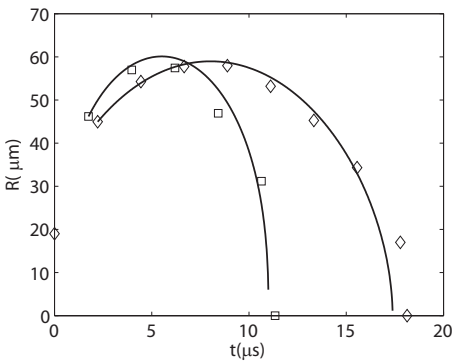

FIG. 3. Fits to the 2D and three-dimensional Rayleigh Pleset equations for $H=0.25$ and $H \to \infty$ for the data shown on Fig. 2. For the 2D equation $R_\infty = 550$ μm, $R_{\max}^{2D} = 58$ μm, and $R_{\max}^{3D} = 57.4$ μm.

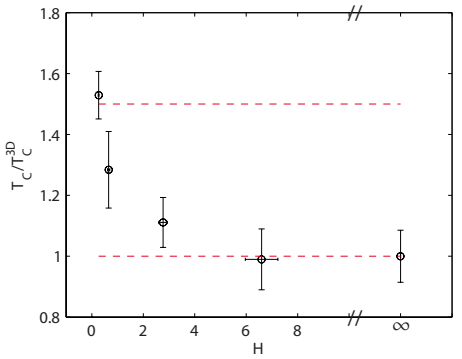

FIG. 4. (Color online) Nondimensionalized collapse time T_C/T_C^{3D} as a function of $H=h/R_{\max}$. Horizontal lines demonstrate the limit cases of a planar and a purely hemispherical bubble.

velocity drops for the planar collapse with $1/r$ (r is the distance to the bubble center) in contrast to the hemispherical bubble where the velocity decays as $1/r^2$.

Figure 3 applies the hemispherical and planar model Eqs. (1) and (2) to the data sets shown in Fig. 2 corresponding to $H\to\infty$ and $H=0.26$, respectively. The initial conditions for solving the ordinary differential equations (ODEs) are obtained from least square fits. We find good agreement between model and experiment, in particular the prolongation of the collapse time is nicely captured. In absolute values, we expect a prolongation of $[\log(R_\infty/R_{\max})]^{1/2}\sim 1.5$ which compares to the experimentally obtained values for $T_C^{3D}=6.4\pm 0.7$ μs and $T_C^{2D}=10.1\pm 1$ μs, i.e., $T_C^{2D}/T_C^{3D}=1.52\pm 0.08$. The ratio T_C^{2D}/T_C^{3D} is plotted in Fig. 4 as a function of H together with the limiting values (horizontal lines) for the planar and hemispherical collapses. Figure 4 shows that the bubble dynamics approaches that of a hemispherical bubble as the height of the microchannel is increased; for $H\approx 7$, the collapse is as fast as in the unconstrained case.

In conclusion, we report on the cavitation bubble dynamics and its collapse behavior as a function of the gap height. Bubbles created close to a rigid boundary and under little vertical constrain, $H\geq 7$, expand and shrink very similar to bubbles in an unconstrained *inviscid* liquid. The fluid velocity drop with $1/r^2$ for most of the oscillation period. Yet in the final stage, we observe loss of the hemispherical symmetry and a jetting toward the lower glass slide. Constraining the bubble increases the oscillation time. For sufficiently small distances, $H\approx 0.26$, the bubble exhibits an essentially planar shrinkage. In the last stage of the collapse, however, when the bubble size is comparable to the gap height, a three-dimensional collapse may set in. Yet, with the resolution and framing speed of the current experiment, we cannot resolve this scenario. Overall, we find a planar shrinkage of the bubble from the maximum radius, indicating a velocity drop with distance as $1/r$. Our findings may have important implications for cavitation in confined geometries and in particular for cavitation powered microfluidic. As an example, we want to mention that for the interaction of cavitation bubbles with cells, it is expected that a more rapid collapse and a stronger shear is created from a hemispherical bubble which may then lead to more severe bubble-cell interaction. A hemispherical bubble collapse may be advantageous for cell lysis and harvesting of intracellular/cytoplasmic content. In contrast, microfluidic devices with a lower height may safeguard cells to induce only temporary pores into membranes, thus assisting drug delivery. Cavitation bubbles are also used to drive microfluidic flows for pumping applications [6,21]. Our results suggest that when modifying the device geometry, the ratio of channel to bubble size should be retained to keep the overall flow pattern. At last, we want to mention current biomedical research where it has been shown that cavitation can induce the formation of vaporous voids to block blood flow for embolotherapy [22]. We suggest that it would be interesting to investigate the ratio of the vessel to bubble size and if it affects the success rate for inducing emboli.

The authors gratefully acknowledge funding through the Ministry of Education, Singapore (Grant No. T208A1238) and Nanyang Technological University through Grant No. RG39/07.

[1] K. R. Rau, A. Guerra, A. Vogel, and V. Venugopalan, Appl. Phys. Lett. **84**, 2940 (2004).
[2] R. Dijkink, S. Le Gac, E. Nijhuis, A. van den Berg, I. Vermes, A. Poot, and C. D. Ohl, Phys. Med. Biol. **53**, 375 (2008).
[3] A. Vogel, Phys. Med. Biol. **42**, 895 (1997).
[4] H. C. Chu, S. Vo, and G. A. Williams, Phys. Rev. Lett. **102**, 204301 (2009).
[5] E. Zwaan, S. Le Gac, K. Tsuji, and C. D. Ohl, Phys. Rev. Lett. **98**, 254501 (2007).
[6] R. Dijkink and C. D. Ohl, Lab Chip **8**, 1676 (2008).
[7] A. N. Hellman, K. R. Rau, H. H. Yoon, S. Bae, J. F. Palmer, K. S. Phillips, N. L. Allbritton, and V. Venugopalan, Anal. Chem. **79**, 4484 (2007).
[8] P. A. Quinto-Su, H. H. Lai, H. H. Yoon, C. E. Sims, N. L. Allbritton, and V. Venugopalan, Lab Chip **8**, 408 (2008).
[9] H. H. Lai, P. A. Quinto-Su, C. E. Sims, M. Bachman, G. P. Li, V. Venugopalan, and N. L. Allbritton, J. R. Soc., Interface **5**, S113 (2008).
[10] T. H. Wu, L. Gao, Y. Chen, K. Wei, and P. Yu Chiou, Appl. Phys. Lett. **93**, 144102 (2008).
[11] S. S. Saliterman, *Fundamentals of BioMEMS and Medical Microdevices* (SPIE Publisher, Bellingham, 2006).
[12] S. Le Gac, E. Zwaan, A. van den Berg, and C. D. Ohl, Lab Chip **7**, 1666 (2007).
[13] P. A. Quinto-Su, V. Venugopalan, and C. D. Ohl, Opt. Express **16**, 18964 (2008).
[14] P. A. Quinto-Su and C. D. Ohl, J. Fluid Mech. **633**, 425 (2009).
[15] E. A. Brujan, G. S. Keen, A. Vogel, and J. R. Blake, Phys. Fluids **14**, 85 (2002).

[16] G. K. Batchelor, *An Introduction to Fluid Dynamics* (Cambridge University Press, London, 1967).
[17] L. Rayleigh, Philos. Mag. **34**, 94 (1917).
[18] T. G. Leighton, *The Acoustic Bubble* (Academic, New York, 1997).
[19] D. Lohse, R. Bergmann, R. Mikkelsen, C. Zeilstra, D. van der Meer, M. Versluis, K. van der Weele, M. van der Hoef, and H. Kuipers, Phys. Rev. Lett. **93**, 198003 (2004).
[20] G. L. Chahine and Ph. F. Genoux, J. Fluids Eng. **105**, 400 (1983).
[21] X. Geng, H. Yuan, H. N. Oguz, and A. Prosperetti, J. Micromech. Microeng. **11**, 270 (2001).
[22] M. L. Fabiilli, K. J. Haworth, N. H. Fakhri, O. D. Kripfgans, P. L. Carson, and J. B. Fowlkes, IEEE Trans. Ultrason. Ferroelectr. Freq. Control **56**, 1006 (2009).